03

Angular dispersion boost of high order laser harmonics interacting with dense plasma clusters

© A.A. Andreev[1,2], L.A. Litvinov[1]

[1] St. Petersburg State University,
199034 St. Petersburg, Russia
[2] Ioffe Institute,
188640 St. Petersburg, Russia
e-mail: litv.lev@gmail.com

Received September 11, 2022
Revised September 11, 2022
Accepted November 28, 2023

Diffraction gratings and photonic crystals are widely used to control light. However, their capabilities are less effective in the case of extreme ultraviolet (XUV) radiation due to the high absorption of the optical material in this frequency range. In this work, we study the possibility of enhancing the angular dispersion of XUV radiation due to scattering by plasma clusters whose dimensions are smaller than the incident radiation wavelength. An analytical model was developed using the plasma Drude dielectric function and the Mie scattering theory in the quasi-static approximation. The resonant parameters of the target for the tenth harmonic of the Ti : Sa-laser are determined, and a significant enhancement of the scattered field in this case compared to the laser one is shown. Under resonance conditions for one cluster, the diffraction of radiation by an array of such clusters is simulated using the CELES code. The results obtained show a significant enhancement of the scattered field in the resonance case for large angles corresponding to the theory of Bragg-Wulf diffraction, which makes it possible to control high harmonics of laser radiation in the XUV range using ionized cluster ga.

Keywords: XUV radiation, ionized cluster gas, femtosecond laser plasma, numerical simulation, phased arrays, light diffraction.

DOI: 10.61011/EOS.2023.02.55797.4114-22

1. Introduction

The interaction of intense coherent radiation with targets of finite size is a well-studied phenomenon, including linearly excited surface plasmon oscillations. Absorption and scattering of incident light in this case can be described with good accuracy using Mie theory, which predicts the existence of a resonance corresponding to multipole oscillations of part of the free electrons of the target relative to positively charged ions. In the resonance mode, the effective excitation of surface plasmons can lead to significant amplification of the cluster field, as well as the field scattered at large angles relative to the original direction of the incident wave.

As is known [1,2], periodic surface lattices and photonic crystals are effective tools for spatial control of light. However, this method is less effective in the case of extreme ultraviolet light because of the high absorption of any material in this frequency range. This work proposes the use of arrays of spherical nanoclusters for directional scattering of hard ultraviolet radiation.

A similar problem for arrays of nano-cylinders as scatterers was investigated earlier [3]. The results obtained showed the efficiency of using nanostructured media in the plasma phase to manipulate the hard ultraviolet. However, manufacturing a set of nano-cylinders with optimal parameters is a complex technological task, whereas arrays of spherical nanoclusters are quite simple to form [4]. The nanoclusters proposed in this work can provide more effective angular dispersion enhancement than nano-cylinders by varying the distance between nanoclusters in three-dimensional space rather than two-dimensional space, and consequently by a more finely tuned spatial configuration of the target.

2. Analytical model

As we know, an intense femtosecond laser pulse of duration τ_L with wavelength $\lambda_L = 830$ nm can be converted to a 10th harmonic pulse with wavelength $\lambda_{10} = 83$, where $\lambda_h = \lambda_L / h$, resulting in a harmonic pulse with intensity $I_h = 1.2 \cdot 10^{14}$ W/cm^2. Total radiation — laser radiation and 10th harmonic radiation interacts with a cluster of radius a.

The interaction results in a dense plasma ball, which can be described within the framework of the Drude model with a dielectric function

$$\varepsilon(\omega_h) = 1 - \left(\frac{\omega_{pe}}{\omega_h}\right)^2 \frac{1}{1 + i\beta_e}, \qquad \omega_{pe} = \sqrt{\frac{4\pi e^2 n_e}{m_e}}, \quad (1)$$

where ω_h — the harmonic frequency considered, ω_{pe} — the electron plasma frequency, e and m_e — electron charge and mass, $n_e = Zn_i$ — electron density, where Z — average degree of ionization, n_i — ion density, $\beta_e = \nu_e/\omega_h$ and ν_e — electron-ion collision frequency in Spitzer approximation.

Under conditions of high-density plasma, the ion density of the cluster is on the order of $n_i = 6 \cdot 10^{22}$ cm^{-3}, and the electron density of the cluster above the critical for a given frequency $n_c = \omega_h^2 m_e / 4\pi e^2$, since otherwise the cluster would be transparent to radiation of that frequency. For 10th harmonic laser radiation $\lambda_h = 83$ nm, we get the condition $n_e > n_c = 1.3 \cdot 10^{23}$ cm^{-3}, which requires an ionization degree $Z > 2$.

We use Mie theory to describe the elastic scattering of electromagnetic waves by particles of arbitrary size in the case of linear interactions, which also allows us to obtain a description of the scattered field and the field inside the scattering object [3,5]. Using the decomposition of a plane wave into vector spherical harmonics, in the case of an $x$polarized incident wave propagating along the z axis, we obtain

$$\mathbf{E}_i = E_0\, e^{i\omega t - ikz}\, \mathbf{e}_x = \sum_{n=1}^{\infty} E_n \left[\mathbf{M}_{o1n}^{(1)} - i\mathbf{N}_{e1n}^{(1)}\right], \qquad (2)$$

$$\mathbf{E}_s = \sum_{n=1}^{\infty} E_n \left[i a_n (ka, m)\, \mathbf{N}_{e1n}^{(3)} - b_n (ka, m)\, \mathbf{M}_{o1n}^{(3)}\right],$$

$$E_n = i^n E_0 \frac{2n+1}{n(n+1)}, \qquad (3)$$

where k — the incident field wave number, $\mathbf{M}_{o1n}^{(1)}$, $\mathbf{M}_{o1n}^{(3)}$ — magnetic vector spherical harmonics, $\mathbf{N}_{e1n}^{(1)}$, $\mathbf{N}_{e1n}^{(3)}$ — electric vector spherical harmonics of [5], the upper index indicates the type of spherical functions in the radial part, the lower index o or e corresponds to the sine or cosine dependence on the azimuthal angle.

The Fourier expansion coefficients (3) on vector spherical harmonics in the case of isotropic medium are scattered field coefficients:

$$a_n(\chi,\ m) = \frac{m\psi_n'(\chi)\,\psi_n(m\chi) - \psi_n'(m\chi)\,\psi_n(\chi)}{m\xi_n'(x)\,\psi_n(m\chi) - \psi_n'(m\chi)\,\xi_n(\chi)}, \qquad (4)$$

$$b_n(\chi,\ m) = \frac{\psi_n'(\chi)\,\psi_n(m\chi) - m\psi_n'(m\chi)\,\psi_n(\chi)}{\xi_n'(\chi)\,\psi_n(m\chi) - m\psi_n'(m\chi)\,\xi_n(\chi)}, \qquad (5)$$

where $\psi_n(\rho) = \rho j_n(\rho)$, $\xi_n(\rho) = \rho h_n(\rho)$ — Riccati-Bessel functions , $h_n = j_n + i\gamma_n$ — spherical Hankel functions of the first kind, $\chi = ka$ — dimensionless radius of the cluster, $m = \sqrt{\varepsilon}$ — the complex refractive index (1).

The specific features of the scattering field coefficients (equality of the denominator to zero) gives a set of resonant electron densities and their corresponding complex scattering coefficients. For $\chi \ll 1$, using the asymptotic approximation [3], we can obtain an analytical expression for the coefficients a_n, the resonance condition taking the form $m^2 = -(n+1)/n$, $n_e = n_c\,(2n+1)/n$ for any natural n. For $\chi \sim 1$, the asymptotic approximation is no longer suitable, since the contribution of the dimensionless radius χ to the resonance position ceases to be negligibly small and its consideration in the corresponding dependence is necessary (Appendix A). In that case, it is necessary to use the expansion of the Hankel and Bessel functions [5].

As a result, it is possible to estimate the resonance parameters of the cluster, in particular the electron density and radius. The resonant value of a_n corresponds to zero in the denominator of the corresponding expression, which corresponds to $|a_n| = 1$, from which we can obtain an expression for the square of the resonant refractive index, which in turn gives an expression for the resonant electron density using (1):

$$m^2(\chi,\ n) = \frac{8n^2(n+1) - (6n+3)\chi^2 - 6n}{2n\chi^2(2n-1)}$$

$$\left[1 + \sqrt{1 - \frac{4n(n-3+4n^2(n+2))(\chi^2+4n-2)\chi^2}{(8n^2(n+1) - (6n+3)\chi^2 - 6n-)^2}}\right], \qquad (6)$$

$$\frac{n_{el}}{n_c} = (1-m^2)\,(1+i\beta_e). \qquad (7)$$

According to (6), (7) the resonance of the scattered field at $\lambda_{10} = 83$ nm corresponds to the resonance electron density $n_{el} = 5.7 \cdot 10^{23}$ cm^{-3} for $\chi + PF = 0.7$ and $n_{el} = 3.9 \cdot 10^{23}$ cm^{-3} for $\chi = 0.3$, which can be achieved on ionized carbon clusters in the state of C^{6+}.

3. Numerical simulation

3.1. Single cluster

As is known [5], the amplitude of the field near the surface of the target can be significantly amplified. We consider the case when the frequency of electron-ion collisions ν_e is much less than the harmonic frequency, so the interaction can be considered collisionless [8]. For this case, the scattered electric field (3) at $\lambda = \lambda_L$ and $\lambda = \lambda_h = \lambda_{10}$ was calculated to compare between resonant and non-resonant cases, the value n_{el} was calculated using (6), (7) at $\lambda_{10} = 83$ nm, $\chi = 0.7$. We see that in the resonant case (Fig. 1, b) the scattered field is a divergent spherical wave and the field amplitude in the vicinity of the cluster is much higher than in the absence of resonance (Fig. 1, a), where the scattering is Rayleigh.

Additionally, the case $\chi = 1.7$ (Fig. 2, a) was calculated and compared to the same situation for a single nanocylinder [3] (Fig. 2, b). It can be seen that the general directions of the scattered field are preserved, we can see weak side orders with deflection angles close to 90° relative to the direction of the incident wave, which is similar to the case of cylindrical symmetry. Differences in the amplitude of scattered waves are due to fundamental differences in the geometry of the cylinder and cluster (Fig. 3) — due to the homogeneity of the cylinder along the axis z the scattered field is attenuated more slowly. The most intense scattering is observed for the direction corresponding to the direction of the incident wave due to structural interference, the scattering efficiency in this direction is about 5%.

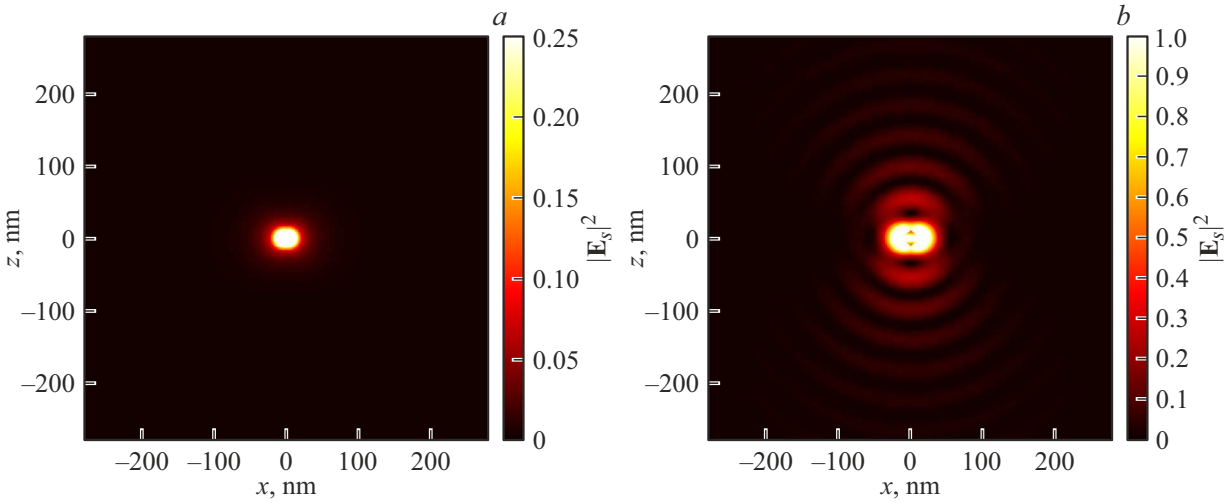

Figure 1. Cluster radius $a = 8.9$ nm; $|\mathbf{E}_s|^2$ in the polarization plane of the incident wave. (a) $\lambda = \lambda_{10} = 83$ nm. (b) $\lambda = \lambda_L = 830$ nm.

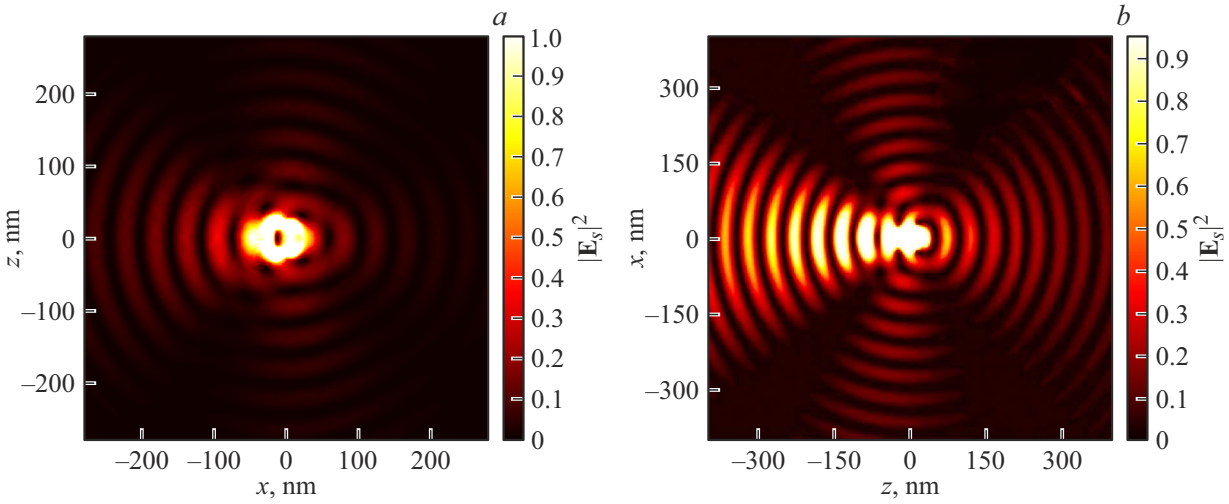

Figure 2. Cluster radius$a = 22.5$ nm ($\chi = 1.7$), $\lambda = \lambda_{10} = 83$ nm; $|\mathbf{E}_s|^2$ is plotted in the polarization plane of the incident wave. Qualitative comparison for the same ka value in the case of cylinders. (a) scattering by a cluster. (b) dissipation by a nano-cylinder [3].

3.2. Multiple clusters

A set of clusters located in a cylindrical gas jet with regular and quasi-regular spatial configurations was considered within the framework of the stationary Mie scattering theory to study the possibility of scattering at large angles of rigid ultraviolet radiation by such structures, in particular corresponding to high order laser harmonics. We use the stationary model due to the quasi-stationarity of the electron density of the target during interaction with laser radiation (Section. 2) within the constraints described (Appendix B).

A primitive cubic lattice with distance between neighboring nodes d was chosen as a regular distribution. The quasi-regular distribution was constructed by introducing random shifts of node coordinates with an arbitrary shift norm in the range $0 \le |\Delta d| \le \eta d$, where $0 \le \eta < 0.5$ — the irregularity degree. In the quasi-regular case, simulations were performed several times in order to average and obtain a generalized picture of the scattered field. CELES [6] program code was used for the calculations.

3.2.1. Geometry of interaction of the radiation beam with clusters The diffraction condition in the case of a three-dimensional regular lattice for elastic scattering in the coordinate system associated with the direction of incident radiation takes the form [7]:

$$\begin{cases} (\mathbf{D}_x,\ \mathbf{e}_{\text{out}} - \mathbf{e}_{\text{in}}) = h^*\lambda \\ (\mathbf{D}_y,\ \mathbf{e}_{\text{out}} - \mathbf{e}_{\text{in}}) = k^*\lambda \\ (\mathbf{D}_z,\ \mathbf{e}_{\text{out}} - \mathbf{e}_{\text{in}}) = l^*\lambda, \end{cases} \tag{8}$$

where h^*, k^*, l^* — the Miller indices represented by integers, $\mathbf{D}_i$ — vector connecting neighboring nodes of the lattice along the direction i, $\mathbf{e}_{\text{in}}$ — unit vector of direction of incident radiation, $\mathbf{e}_{\text{out}}$ — unit vector of direction of

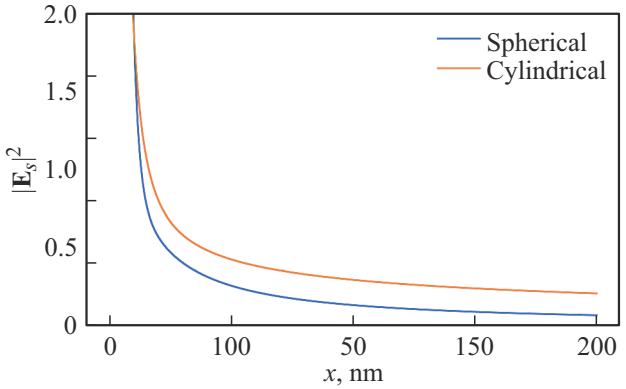

Figure 3. The modulus of the first term $|\mathbf{E}_s|$ depending on the coordinate x ($\theta = 0°$, $\varphi = 0°$) for spherical and cylindrical cases, the dimensionless radius of the cluster $\chi = 1.7$.

radiation passed. Turning to the spherical coordinates associated with $\mathbf{e}_{\text{in}}$ such that in the Cartesian representation $\mathbf{e}_{\text{in}} = \mathbf{e}_z$, equations (8) can be transformed as follows, given that $||\mathbf{D}_x| = |\mathbf{D}_y| = |\mathbf{D}_z| = d$ for the considered cubic lattice:

$$\begin{cases} \cos\theta_0 \sin\Delta\theta \cos(\Delta\varphi - \varphi_0) - \sin\theta_0 (\cos\Delta\theta - 1) = \dfrac{h'\lambda}{d} \\ \sin\Delta\theta \sin(\Delta\varphi - \varphi_0) = \dfrac{k'\lambda}{d} \\ \sin\theta_0 \sin\Delta\theta \cos(\Delta\varphi - \varphi_0) + \cos\theta_0 (\cos\Delta\theta - 1) = \dfrac{l'\lambda}{d}, \end{cases} \tag{9}$$

where Δ, θ, $\Delta\varphi$ — angles characterizing the deviation of the direction of the diffracted radiation relative to the incident, θ_0, φ_0 — angles characterizing the rotation of the target (lattice) in space, h', k', l' — new Miller indices (Fig. 4). Using (9), we can obtain the angular distribution of the diffracted radiation at given initial parameters d, λ, θ_0, φ_0.

3.2.2. Scattering of monochromatic radiation In order to check the model validity, let us calculate the stationary interaction in the regular case for various parameters of the lattice and the width of the Gaussian beam $w = 800$ nm, the radius of the cylinder limiting the lattice (the radius of the gas jet) $r_{\text{gas}} = a + 12d \approx 2\,\mu$m, where the multiplier at d —is the number of lattice nodes between the central axis and the boundary of the cylinder. Although it is virtually impossible to obtain a Gaussian beam of the 10-th harmonic Ti:Sa laser with a width of 800 nm in real conditions, due to the stationarity of the calculations, the ratio w / r_{gas} can be correctly scaled at $w \ll 2r_{\text{gas}}$. The small value w used in this case speeds up the calculations, but does not fundamentally change their result.

The difference in scattering in the resonant and non-resonant case is shown in Fig. 5 — the square of the scattered field amplitude is more than 10 times greater in the resonant case than in the non-resonant case. Also, in the absence of resonance, there are no orders of diffraction other than zero, which follows directly from the restriction on the maximum Miller index in (9).

Let us determine the most intense scattering directions using the following integral characteristic:

$$E_{\text{int}}(\eta,\ \lambda,\ V(\Delta\theta,\ \Delta\varphi),\ E_0,\ \varphi_0,\ \theta_0) = \int\limits_{V(\Delta\theta,\ \Delta\varphi)} |\mathbf{E}_s(\eta,\ \lambda,\ E_0,\ \varphi_0,\ \theta_0)|^2 dV. \tag{10}$$

Here, E_{int} is the integral energy density of the scattered field in the area of space V for the lattice having irregularity η, i. e. is the energy scattered by the grating into the area V, λ represents the wavelength of the incident field, E_0 — the amplitude, the angles φ_0, θ_0 — set the target position in space according to (Fig. 4). The area V must be set so as to characterize some direction in space, and usually for this purpose a cone-shaped area formed by some solution of the solid angle $\delta\Omega$ and the direction using angles $\Delta\theta$, $\Delta\varphi$ is used. For the problem under consideration, it is necessary to exclude the near-field from the calculation, due to which we impose an additional restriction of the V area by the inner spherical layer of space with boundaries b_1 and b_2, where b_2 — the boundary of the numerical simulation area, b_1 — larger than the radius of the sphere described around the target. Although the gas jet is an extended object, only a segment of it is used in the simulation, since the incident beam is limited and the scattering field weakly depends on the parts of the jet distant from the beam incidence area, which allows describing a corresponding circle around such a segment.

The intersection of the conic area and the spherical layer away from the target can be approximated by a cylinder, considering $r_{\text{cyl}} \approx 0.5\, b_2 \cdot \delta\Omega$, where r_{cyl} is the radius of the cylinder. In this case, using the auxiliary vector $\mathbf{c}$ we obtain the area V (Fig. 4, *a*):

$$\mathbf{c} = \mathbf{c}(\mathbf{x},\ \Delta\theta,\ \Delta\varphi) = \begin{pmatrix} c_x \\ c_y \\ c_z \end{pmatrix} = M_y(\Delta\theta)\, M_z(\Delta\varphi)\, \mathbf{x},$$

$$\mathbf{x} = \begin{pmatrix} x \\ y \\ z \end{pmatrix}, \tag{11}$$

$$V(\Delta\theta,\ \Delta\varphi) = \left\{ \mathbf{x} \in b_1^2 \le |\mathbf{x}|^2 \le b_2^2 : c_x^2 + c_y^2 \le r_{\text{cyl}}^2, \ \right\}, \tag{12}$$

where $M_y(\Delta\theta)$ is the rotation matrix around the Cartesian axis y by the angle $\Delta\theta$ counterclockwise, $M_z(\Delta\varphi)$ — the rotation matrix around the Cartesian axis z by the angle $\Delta\varphi$ counterclockwise. The fraction of radiation deflected in a particular direction E_{frac} can be determined using the following expression:

$$E_{\text{frac}}(\eta,\ \lambda,\ V,\ E_0,\ \varphi_0,\ \theta_0) = \frac{E_{\text{int}}(\eta,\ \lambda,\ V,\ E_0,\ \varphi_0,\ \theta_0)}{\int\limits_{V_0} |\mathbf{E}_i(\lambda,\ E_0,\ w)|^2 dV}, \tag{13}$$

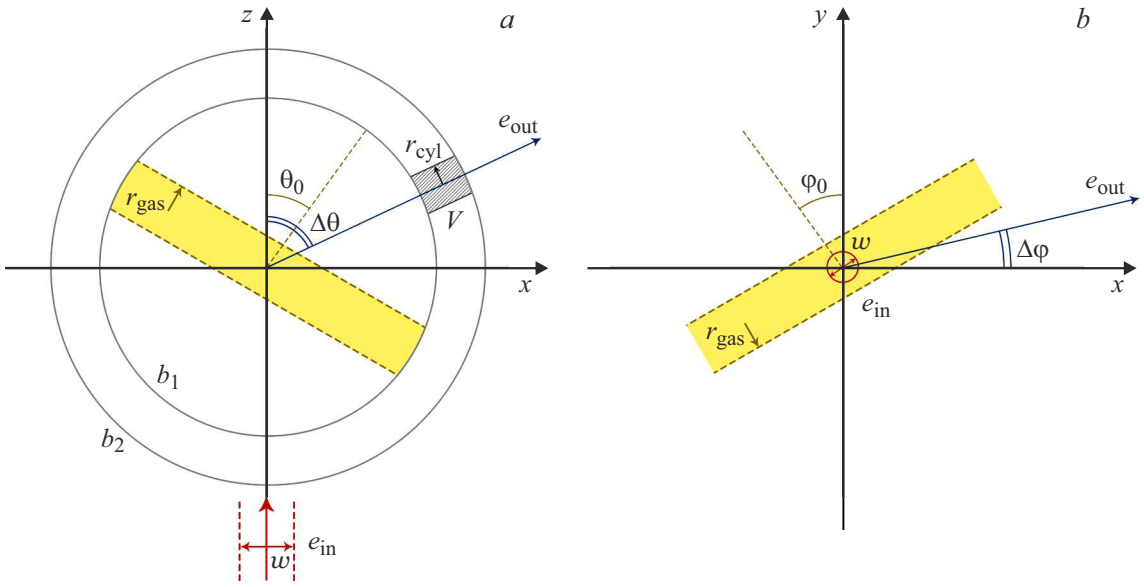

Figure 4. General scheme of interaction of incident radiation with the lattice: θ_0, φ_0 — characterize the angles of rotation of the target in space, $\Delta\theta$, $\Delta\varphi$ — angles of deviation of direction of the diffracted radiation relative to the incident, r_{gas} — radius of gas jet representing the target, w - diameter of Gaussian beam of incident radiation. (a) projection onto the plane xz. (b) projection onto the plane xy.

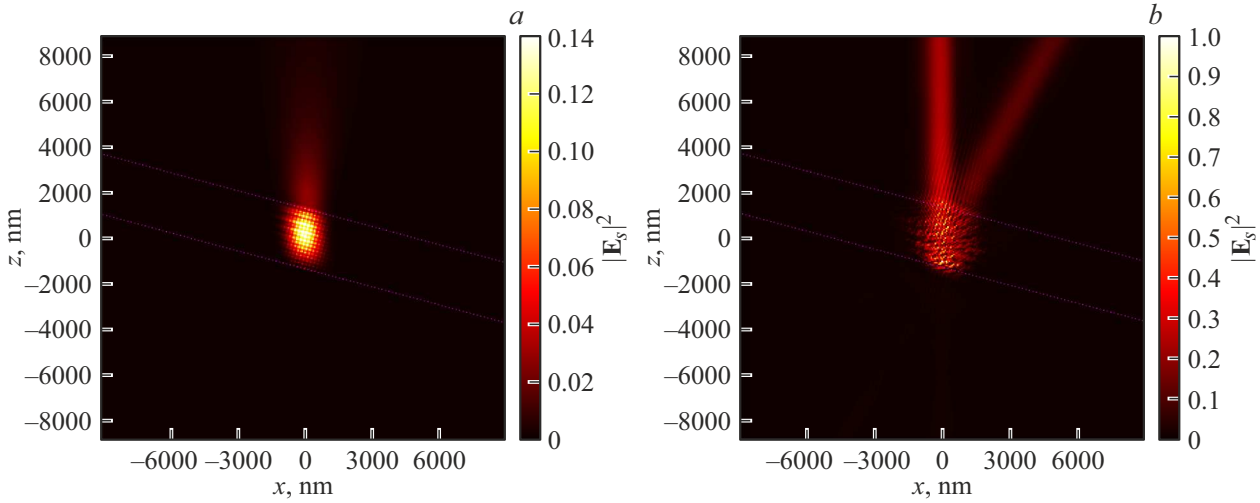

Figure 5. $|\mathbf{E}_s|^2$ in the polarization plane, the cross section $\Delta\varphi = 0°$ — scattering of a Gaussian beam on a layer of quasi-regularly arranged clusters of radius $a = 20$ nm, $\theta_0 = 15°$, $\varphi_0 = 0°$. The gas layer boundaries are marked in magenta. The amplitude of the scattered field is normalized to the maximum value in the case of the 10th harmonic. (a) $\lambda = \lambda_L = 830$ nm. (b) $\lambda = \lambda_{10} = 83$ nm.

where $V_0 = \{\mathbf{x} \in b_1^2 \leq |\mathbf{x}|^2 \leq b_2^2\}$ — far zone of the simulation area.

We also construct integer solutions for h', k', l' with given θ_0, φ_0 in the axes $\Delta\varphi$, $\Delta\theta$ using (9) (Fig. 6, a). The graphs in Fig. 6 are diagrams in polar coordinates ($\Delta\theta$, $\Delta\varphi$), i. e., projections of the sphere surface bounded by some range of angle $\Delta\theta$, onto a plane. This construction method is more convenient for depicting the spatial distribution of scattered radiation, and is also more natural for mapping integer solutions to the Miller indices (9), since they are then sets of rings on a sphere. According to the results obtained, we can see that the most intense diffraction directions by E_{int} correspond to the closest location of the curves corresponding to the integer values of the Miller indices. In this case, the scattering efficiency in the most intense directions with respect to the incident field reaches $E_{frac} = 0.2$ ($\Delta\varphi = 0°$, $\Delta\theta = 30°$), which corresponds to 20%.

Let us consider the effect of irregularity on the most intense directions of the scattered field, i. e., the dependence (10) on the irregularity of the lattice η. For this purpose, the scattering in the case of a quasi-regular lattice at different parameters and irregularity η from 0 to 0.5 is simulated (Fig. 7).

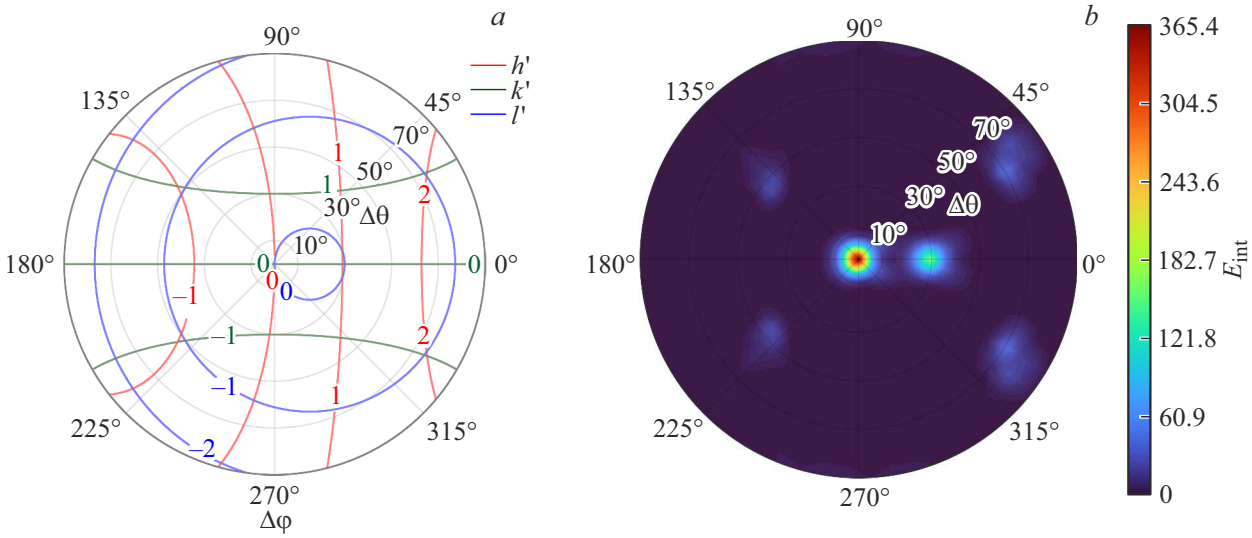

Figure 6. Scattering of the 10th harmonic with lattice parameters $a = 20$ nm and $d = 2\lambda_{10}$, $\varphi_0 = 0°$, $\theta_0 = 15°$, $\lambda = \lambda_{10} = 83$ nm, range of construction $\Delta\theta \in [0,\ \pi/2]$. (*a*) solution (9) in integer Miller indices. (*b*) E_{int} till (10).

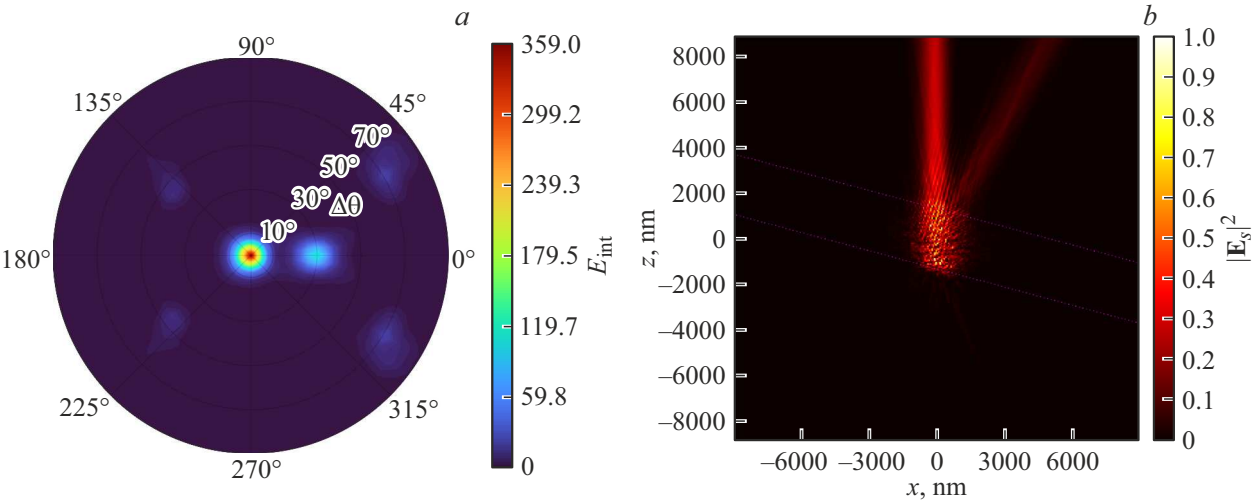

Figure 7. Gaussian beam scattering on a layer of quasi-regularly arranged clusters of radius $a = 20$ nm, $\theta_0 = 15°$, $\varphi_0 = 0°$. (*a*) E_{int} by (10), $\eta = 0.1$. (*b*) $||\mathbf{E}_s|^2$ in the polarization plane, section $\Delta\varphi = 0$, $\eta = 0.1$.

Using a normalized version (14) of the integral characteristic (10) described earlier, the corresponding dependence on irregularity was constructed (Fig. 8). With increasing irregularity, the most intense directions, except for the zero direction, are significantly attenuated, up to 80% relative to the regular case, while the overall scattering pattern in different directions flattens out until it is almost homogeneous at $\eta \to 0.5$ (Fig. 7).

$$E_{int}^{norm}(\eta,\ \lambda,\ V,\ E_0) = \frac{E_{int}(\eta,\ \lambda,\ V,\ E_0)}{E_{int}(0,\ \lambda,\ V,\ E_0)}. \qquad (14)$$

The dependence of the scattering intensity directions on $\Delta\theta$ as a function of θ_0 in the cross section $\Delta\varphi = 0$ was considered. The value $\varphi_0 = 0$ was taken, since any nonzero value of this angle essentially rotates the angular distribution by the same angle. The result obtained fully correlates with the previously obtained formulas (9) — the positions of the spots corresponding to the most intense scattered field directions other than zero in Fig. 9, *b* correspond to the intersections of the lines of the integer values of the Miller indices in Fig. 9, *a*.

The most intense scattering direction corresponding to $\theta_0 = 15°$, $\Delta\theta = 30°$ was chosen, for which the dependence of the value of the previously constructed integral characteristic (10) on the cluster radius was considered (Fig. 10). We can see the presence of a global maximum in the constructed dependence, which allows to talk about the existence of the optimal value of the radius for the corresponding direction.

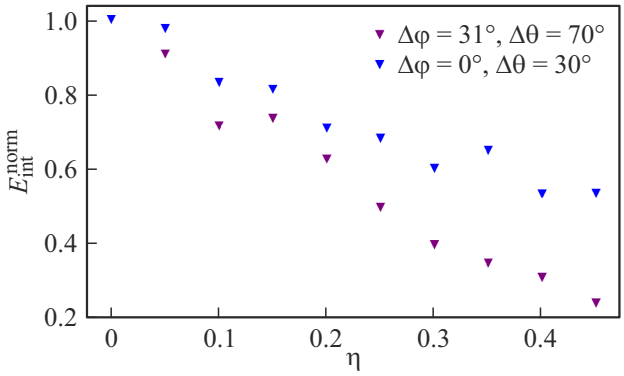

Figure 8. Scattering attenuation as a function of lattice irregularity.

3.2.3. Scattering of the wave packet Earlier, we considered the scattering of monochromatic radiation, but in fact, during the conversion of the main pulse with a duration of τ_L a set of harmonics with an unknown distribution is generated. For simplicity, consider a wave packet with some half-width localized near the 10th harmonic. Its amplitude in time is described by a Gaussian function (15), where τ_h — the total width of the transformed harmonic pulse. Let us decompose the amplitude of the wave packet into a Fourier series:

$$A_h(t) = E_h \exp\left(-\frac{t^2}{(\tau_h / 2)^2}\right), \tag{15}$$

$$A_h(t) = \frac{\sqrt{\pi}}{2} + \sum_{j=1}^{\infty} A_j \cos(\omega_j t),$$

$$\omega_j = \frac{2\pi j}{\tau_L} = \frac{c}{\lambda_j}, \quad \lambda_j = \frac{\lambda_L}{j}, \tag{16}$$

$$A_j = \frac{1}{\tau} \int_{-\tau}^{\tau} E_0 \exp\left(-\frac{t^2}{(\tau_h / 2)^2}\right) \cos(\omega_j t) dt. \tag{17}$$

In order to plot the scattering diagram of the wave packet, we used a new integral characteristic determined with the obtained Fourier coefficients (18). Such a characterization is reasonable for describing scattering directions because of the additivity of energy as a quantitative characteristic. The V area in this case is similar to that used for the previous integral characteristic (12):

$$\mathscr{E}_{\text{int}}(V,\ \eta,\ \varphi_0,\ \theta_0) = \sum_{j\,=\,N_1\,>\,0}^{N_2} E_{\text{int}}(\eta,\ \lambda_j,\ V,\ A_j,\ \varphi_0,\ \theta_0). \tag{18}$$

Let us find the most intense scattered field directions for a lattice with resonance parameters defined using the monochromatic model: $d = 2\lambda_{10}$, cluster radius $a = 20$ nm, $\theta_0 = 15°$, $\varphi_0 = 0°$. Harmonics in the wave packet from 8th to 12th, i. e., $N_1 = 8$, $N_2 = 12$ in (18), the Gaussian pulse has a duration of $\tau_h \approx 30$ fs. The obtained result is comparable with the monochromatic case with similar lattice parameters, direction and energy of incident radiation.

At the zero diffraction maximum corresponding to the passed radiation, we have identical values by virtue of (9) when $h' = k' = l' = 0$ and the same incident field energy. The diffraction maxima of the other orders are attenuated and blurred (Fig. 11). This is due to the fact that the harmonics in the wave packet, other than the 10th, no longer correspond to the given resonance parameters, then the directional energy corresponding to these harmonics is redistributed, which also shows (9). In particular, the relative efficiency E_{frac} of the first diffraction maximum ($\Delta\varphi = 0°$, $\Delta\theta = 30°$) weakens from 0.3 to 0.1.

3.2.4. Conditions for optimal scattering of XUV radiation in a given direction As noted earlier, the main goal of this work is directional scattering of radiation in the XUV range. For this purpose, we propose a cluster target with a quasi-regular structure in the general case, whose parameters must be chosen based on the conditions, i. e. the wavelength of the most intense spectral component of the wave packet or monochromatic radiation λ, and the desired deflection angles $\Delta\varphi$, $\Delta\theta$ relative to the direction of the incident radiation.

First of all, it is necessary to estimate the radius of clusters a using the analytical model (6). The resulting value will be an initial estimate of the resonance value of the cluster radius when the material is known in advance. Next, it is necessary to choose the distance between clusters d. Setting large d for the lattice (multiples of the incident field wavelength in the case of monochromatic radiation or the wavelength of the most intense spectral component in the case of a wave packet) increases the number of diffraction maxima realized, reducing efficiency (the ratio of cluster diameter to cluster spacing decreases) but also increasing the range of angles to which radiation can potentially be deflected. Small d provides the most intense scattering in the near orders of diffraction, but causes a limited set of angles located near the intersections of the curves of the integer solutions of Laue's system of equations, as can be clearly seen in Fig. 9, *b*.

Formulas (9) allow you to estimate the position of such intersections and choose the most appropriate value d depending on the required deflection angles $\Delta\varphi$, $\Delta\theta$. After that, it is necessary to calculate the scattered field, with which the integral characteristic E_{int} (10) for a given geometry and range of cluster radius $a \pm 20\%$ should be calculated in order to refine the initial estimate and take into account diffraction effects in the near and middle zone.

The presence of η irregularity in the lattice inevitably causes the diffraction maxima to blur and weaken, which must be taken into account when evaluating scattering efficiency using (13).

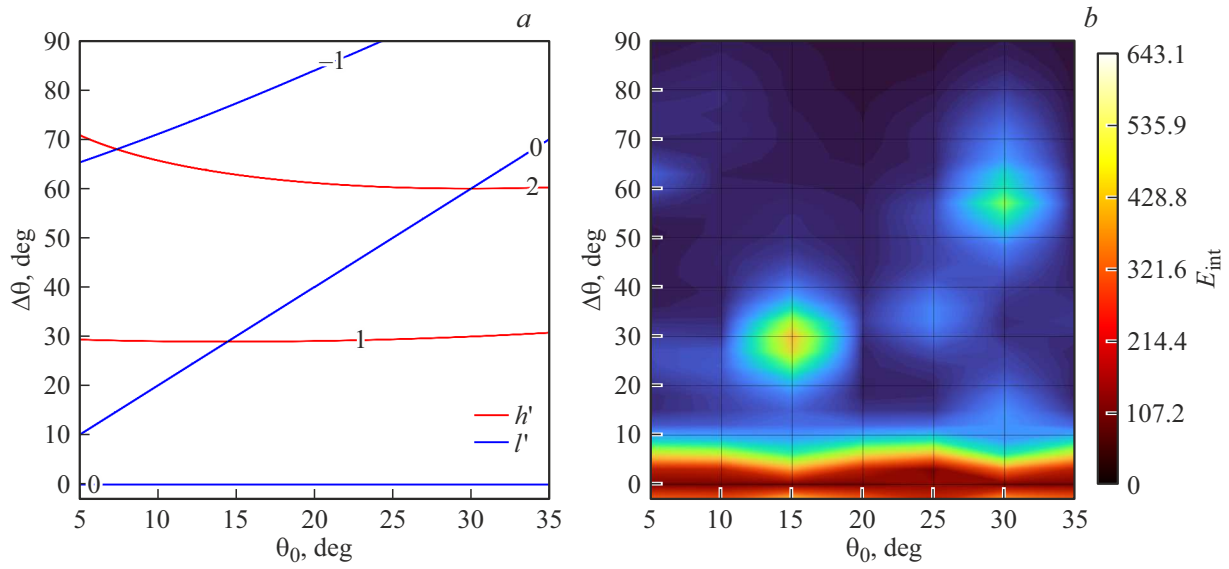

Figure 9. Scattering of the 10th harmonic at different angles θ_0, $\varphi_0 = 0$, $\Delta\varphi = 0$, $a = 20$ nm, $d = 2\lambda_{10}$. On (a) $k' = 0$ for any θ_0 and $\Delta\theta$. (a) E solution (9) in integer Miller indices. (b) E_{int} by (10).

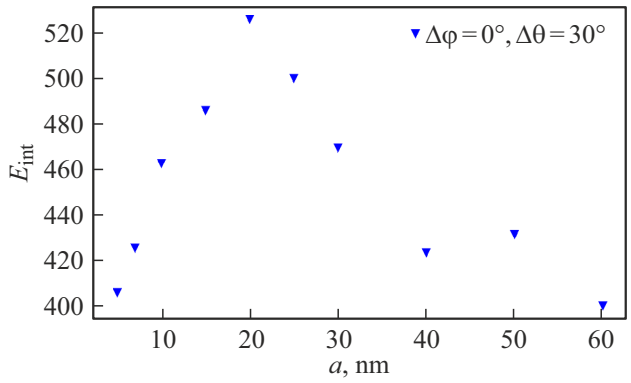

Figure 10. Scattering attenuation as a function of cluster radius.

4. Conclusion

A periodic structure of dense plasma clusters was found to be a suitable element for directional effective scattering of XUV radiation. Since many spherical scatterers require costly calculations in three-dimensional space, a stationary model was proposed and the range of cluster radii within which the electron density is quasi-stationary during interaction with the external field was determined. When the ionization is such that the concentration of electrons is close to the resonance concentration for a given initial parameter, the scattering efficiency increases significantly and reaches several percent in the case of a single cluster. For multiple clusters, the efficiency of angular dispersion increases with the number of clusters and can reach several tens of percent in the case of certain directions.

The resulting angular distributions of diffraction maxima for scattering with many regularly spaced clusters are well described by Laue's theory, and introducing a small irregularity in the cluster distribution weakens the most intense diffraction directions other than the direction of the passed radiation by no more than 25%. In the case of non-monochromatic radiation, the gain efficiency of the angular dispersion decreases according to the width of the spectral distribution of the interacting field.

Conflict of interest

The authors declare that they have no conflicts of interest.

Appendix

A. Asymptotic approximation of the scattered field coefficients and approximation by series expansion

Fig. 12 shows the dependence of the scattering coefficient on the electron density for $\chi = 1.5$ in the asymptotic approximation and the Hankel and Bessel function series expansion approximation. One can clearly see a significant difference in the shape and position of the curves for different n when using the asymptotic approximation, while the approximation by series expansion has only inaccuracy in the form of a shift, which tends to zero with increasing order n.

B. Rationale for the stationary model

In the general case, calculating the interaction of a high-intensity laser pulse with a group of dense spherical clusters located in three-dimensional space requires long and complex non-stationary calculations due to the fact that

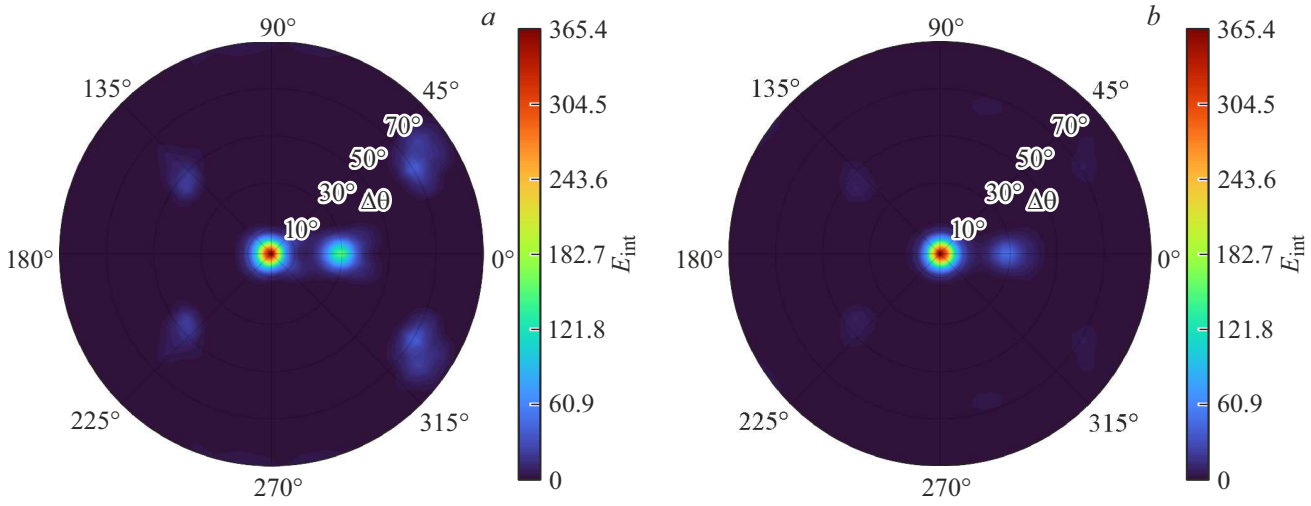

Figure 11. Angular scattering diagram at $\theta_0 = 15°$, $\varphi_0 = 0°$, $d = 2\lambda_{10}$, cluster radius $a = 20$ nm. (a) scattering of the 10th harmonic. (b) wave packet scattering.

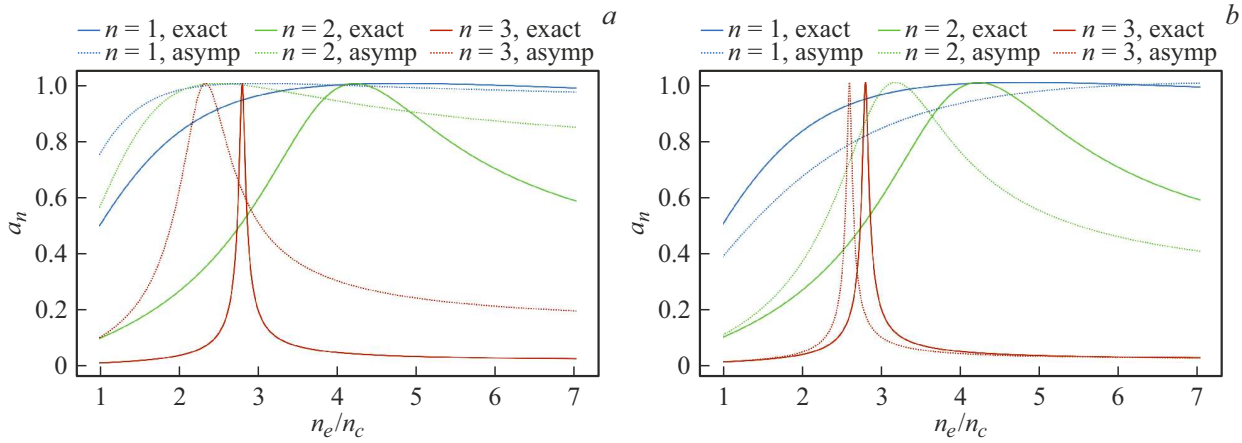

Figure 12. Coefficients of spherical harmonics at $\beta_e = 0$, $\chi = 1.5$. The curves „exact“ correspond to the exact values of the scattered field coefficients. (a) asymptotic approximation. (b) decomposition in series up to the first term.

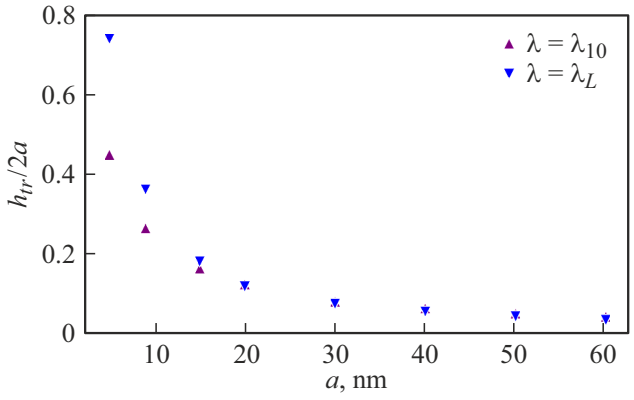

Figure 13. Asymptotics of the average total thickness of the transition layer at $0 \le t \le 10T$ with respect to the radius of the target. n_c used in the construction corresponds to the critical density for wavelength $\lambda = \lambda_{10}$.

the electron density distribution of clusters as a result of interaction with the laser pulse changes over time.

To verify the magnitude of the electron density change in the case under consideration, we simulated the evolution of the electron density distribution in the one-dimensional space of a single cluster. The LPIC++ [8] code was used for the simulation. Two pulses were considered as sources: a primary frontal linearly polarized laser pulse with wavelength $\lambda_L = 830$ nm, duration τ, pulse amplitude envelope shape in time $\sin^2(t)$, intensity $I_L = 10^{18}$ W/cm^2 and transformed with wavelength $\lambda_{10} = 83$ nm, duration τ and intensity $I_h = 10^{14}$ W/cm^2. The period of laser radiation corresponding to the laser harmonic is $T = \lambda_L / c \approx 2.8$ fs, so the pulse length in the simulation was taken $\tau = 10T = 28$ fs, simulation time $t = 20T = 56$ fs. The plasma is represented by 2000 particles in each cell occupied by a target located in the center of a box of width $w_{\text{box}} \approx 3\lambda_{10}$; the electron density of the target

in critical units is $n_{el} = 4.2n_c$. We also considered the interaction with the first harmonic, for which $\lambda_L = 830\,\text{nm}$, $I_L = 10^{18}\,\text{W/cm}^2$. Single clusters of radius a from 9 to 60 nm were taken as targets.

Based on the obtained simulation results, the average total thickness of the transition layer during the interaction with the external pulse h_{tr} as a function of the target radius a was calculated (Fig. 13). The quasi-stationary condition in this case takes the form $h_{tr} \ll 2a$, which holds for $a \geq 20\,\text{nm}$. Thus, when using stationary calculations to estimate angular scattering, it is acceptable to use only clusters with a radius of 20 nm or greater.

References

[1] X. Lin, X. Zhang, K. Yao, X. Jiang. J. Opt. Soc. Am. B, **31** (5), 1145 (2014). DOI: 10.1364/JOSAB.31.001145
[2] B.W. Batterman, H. Cole. Rev. Mod. Phys., **36** (3), 681 (1964). DOI: 10.1103/RevModPhys.36.681
[3] Z. Lécz, A.A. Andreev. Optics Express, **28** (4), 5355 (2020). DOI: 10.1063/1.5123542
[4] V.P. Kraynov, M.B. Smirnov. UFN, **170** (in Russian). (9), 969 (2000). DOI: 10.3367/UFNr.0170.200009b.0969
[5] K. Boren, D. Huffman. *Pogloscheniye i rasseyaniye sveta malymi chastitsami* (Mir, M., 1986) (in Russian).
[6] A. Egel, L. Pattelli, G. Mazzamuto, D. Wiersma, U. Lemmer. J. Quant. Spectrosc. Radiat., **199**, 103 (2017). DOI: 10.1016/j.jqsrt.2017.05.010
[7] Ch. Kittel. *Vvedenie v fiziku tverdogo tela,* (Fizmatgiz, 1962). (In Russian).
AIP Conference Proceedings (AIP, 1998), vol. 426, p. 141. DOI: 10. 1063/1.55199

Translated by Y.Deineka